Diffusion of Xe and Kr implanted at low concentrations in UO_2 as a function of temperature – An experimental study

M Gérardin, E Gilabert, D Horlait, M-F Barthe, G Carlot

Diffusion of Xe and Kr implanted at low concentrations in UO2 as a function of temperature – An experimental study

M. Gérardin, E. Gilabert, D. Horlait, M-F Barthe, G. Carlot

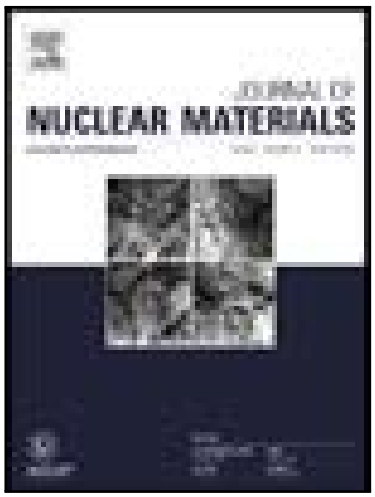

Diffusion of Xe and Kr implanted at low concentrations in UO_2 as a function of temperature – An experimental study

M. Gérardin , E. Gilabert , D. Horlait , M-F. Barthe , G. Carlot

PII: S0022-3115(23)00243-X
DOI: https://doi.org/10.1016/j.jnucmat.2023.154476
Reference: NUMA 154476

To appear in: *Journal of Nuclear Materials*

Received date: 2 August 2022
Revised date: 8 November 2022
Accepted date: 20 April 2023

Please cite this article as: M. Gérardin , E. Gilabert , D. Horlait , M-F. Barthe , G. Carlot , Diffusion of Xe and Kr implanted at low concentrations in UO_2 as a function of temperature – An experimental study, *Journal of Nuclear Materials* (2023), doi: https://doi.org/10.1016/j.jnucmat.2023.154476

Diffusion of Xe and Kr implanted at low concentrations in UO_2 as a function of temperature – An experimental study

M. Gérardin[1,2*], E. Gilabert[3], D. Horlait[3], M-F. Barthe[4], G. Carlot[1]

[1] *CEA, DEN, DEC, F-13108 Saint Paul lez Durance Cedex, France*
[2] *Université de Lorraine, GeoRessources, CNRS, F-54000 Nancy, France*
[3] *Université de Bordeaux, CNRS, LP2I Bordeaux, UMR5797, F-33170 Gradignan, France*
[4] *CEMHTI/CNRS, Université d'Orléans, 3A rue de La Férollerie, F-45071 Orléans CEDEX 2, France* Corresponding Author : marie.gerardin@protonmail.com*

Abstract
Fission gases production and release have a large impact on uranium dioxide fuel performance. To predict fuel properties in pile, a better understanding of the fission gas behaviour in uranium dioxide is needed. UO_2 samples were implanted with Xe or Kr at low doses to avoid trapping by irradiation defects and/or gas clusters. The release rates of Xe and Kr were studied at temperatures ranging up to 1400°C. Results show an excellent agreement with the substantial literature on xenon diffusion in irradiated UO_2.

1 Introduction

Fission of uranium and plutonium produces high levels of rare gases such as xenon or krypton, which are particularly insoluble. Therefore, they tend either to be released into the free volume of the fuel pin, increasing the pressure inside the cladding, or to form small nanometre size clusters inducing fuel swelling and participating to its fracturing and incidental heat diffusivity decreasing [1]–[4]. To prevent cladding failure and maintain fuel performance, a better understanding of gaseous fission product transport and release is essential.

The basic diffusion properties are determined by the interaction between the location of atoms in the lattice and the defects induced mainly by irradiation or temperature. Calculations by density functional theory (DFT) [5]–[16] and molecular dynamics (MD) with empirical potentials [17]–[21] have shown that large fission gas atoms such as xenon prefer uranium vacancy related defects. According to calculations by DFT+U in stoichiometric $UO_{2.00}$ [15], [16], xenon and krypton atoms are likely to be located in a charged di-vacancy UO (V_{UO}^{-} or V_{UO}^{2-}) and their migration involves an additional uranium vacancy, fully charged (V_U^{4-}). The authors reported that for this mechanism, the activation energy ranges from 2.93 to 7.80 eV and the pre-exponential factor lies in the range of $4.3\text{x}10^{-8}$ to $5.0\text{x}10^{-3}$ m^2/s. They also reported that the location and the migration mechanism change with O/U stoichiometry. Furthermore, the recent work of Perriot et al. [22] shows that the diffusion of xenon is dominated by Xe in V_{UO} at high temperatures and V_{U_2O} at lower temperatures. For comparison with experimental studies, the results of their simulation are presented in the Fig. 4.

Experimental data on fission gas migration rely on gas release measurements mainly in post-irradiation annealing. Xenon and krypton thermal diffusion in UO_2 depends on (i) the stoichiometry [20], [23]–[26]: it increases with stoichiometry for >2.021 values and decreases when below 1.997 and (ii) the burn-up [27]–[29]: it decreases from 10^{22} fission/m^3 to reach a saturated state at 10^{24} fission/m^3. The apparent decrease of the diffusion coefficient with the burn-up has been explained by a trapping effect [27]. This behaviour was recently highlighted on UO_2 samples implanted with low concentrations of xenon or krypton [30]. The apparent decrease on the diffusion coefficient with the increasing fluence is explained by the trapping of gas atoms by the defects formed during the

implantation process. Those defects could be small vacancy clusters or to a lesser extent, nanometer size cavities. This mechanism appears between $1.2x10^{13}$ and $5x10^{13}$ i/cm^2 for Xe implanted at 800 keV in UO_2 and the fraction of gas trapped increases with the fluence.

To define the intrinsic diffusion coefficient of heavy rare gas in UO_2, experiments should be performed on stoichiometric $UO_{2.00}$ irradiated with a burn-up lower than 10^{22} fission/m^3 or implanted with a fluence $\leq 1.2x10^{13}$ i/cm^2. On post-irradiation studies, Arrhenius plots (see Fig. 4) obtained under these conditions [23], [31]–[33] show an agreement on the value of the activation energy of xenon of supposedly intrinsic diffusion, lying between 2.1 and 3.9 eV. The pre-exponential factor however varies from 2.10^{-12} and 5.10^{-4} m^2/s. One study on krypton thermal diffusion performed by Auskern [34] outputs E_a and D_0 values in the same ranges than those for xenon diffusion (3.2 eV and $4.9x10^{-8}$ m^2/s), supposing that Kr and Xe diffuses via the same mechanisms in $UO_{2.00}$ irradiated with a low burnup. This is supported by experimental data on Xe and Kr releases from implanted UO_2 annealed at 1300°C [30]. For the vast majority of experimental works, the values of E_a and D_0 were obtained by applying the Booth sphere model [35] on the measurements of the gas release rates. This model represents the microstructure by independent spheres and the release occurs by gas diffusion to the surface of these equivalent spheres. However, this representation of the microstructure has been questioned [34]. This model does not consider the burst release, described as a high release occurring during the first tens of minutes of annealing that could comprise more than half of the total gas release [4]. Moreover, the Booth model does not take into account the trapping effect along the gas diffusion path assumed in the literature [28], [36]–[43], and experimentally highlighted by Carter et al. [43] and our previous work [30].

This work proposes to determine the diffusion coefficient as a function of the temperature with a diffusion model based on Fick's second law, which accounts for the burst release and the trapping mechanisms occurring during ion implantation and along the gas diffusion path. This model was described in our previous work [30] on the fluence dependence on rare gases diffusion at 1300°C. In the present study, annealing experiments at various temperatures ranging from 600 to 1400°C are performed on samples implanted with low doses to avoid the formerly evidenced trapping effect during implantation. Arrhenius laws of xenon and krypton implanted in UO_2 will be presented and discussed in the light of previous experimental studies.

2 Experimental

Unirradiated fuel pellets are cut in discs (~500 µm thickness), polished and annealed at 1700°C during 24 hours under a reducing atmosphere Ar-5%H_2. As this treatment causes grooves at the grain boundaries, we performed a second polishing treatment with a colloidal silica suspension (OP-U by *Struers* [44], [45]). Finally, to remove polishing defects induced by OP-U treatment, a second annealing is performed at 1400°C during 4h under Ar-5%H_2. Grain size is evaluated at 7.6 ± 1.5 µm. The stoichiometry (O/U) of the samples is evaluated between 1.9996 and 1.9998 by a calculation based on TAF-ID (Thermodynamics of Advanced Fuels – International Database) [46].

As prepared samples were implanted at room temperature with 800 keV ^{129}Xe or 500 keV ^{83}Kr at low fluences (between $1.4x10^{11}$ and $2x10^{12}$ i/cm^2) at IP2I (Institut de Physique des 2 Infinis de Lyon - France) using the implantor IMIO400. The fluence was measured using Thermo-Desorption Spectrometry (described below) by melting 4 Al foils that were placed aside the UO_2 samples during ion implantations on each sample holder. We evaluated the mean value of the fluence for each sample holder. The fluence of each sample was fixed to this value (reported in Table 1) with an estimated error of 10%.

The profiles of gas content and atomic displacements (dpa) induced by these implantations are calculated using the SRIM simulation code [47] ("Quick calculation damage" with threshold displacement energies for oxygen and uranium set to 20 and 40 eV respectively [48], [49]). From SRIM calculations, the projected range R_p of xenon and krypton is 148 nm where the gas concentration reaches a maximum of about 0.08 ppm at 10^{11} i/cm^2. These implantations create a damage area on the first 250 nm from the surface (Fig. 1).

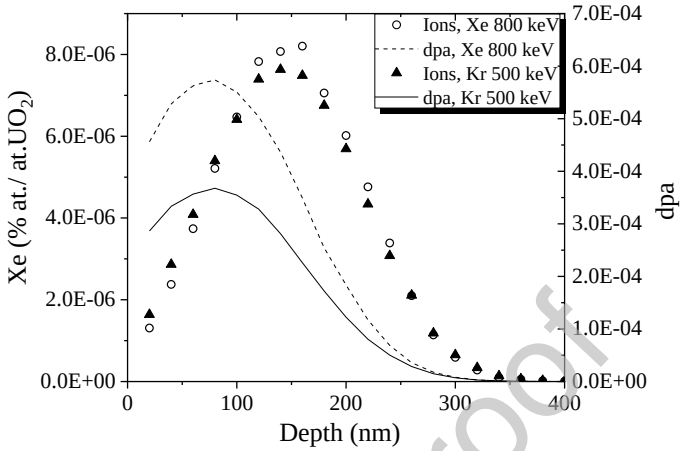

Fig. 1 - Depth profiles based on SRIM calculations [47] of 800 keV xenon or 500 keV krypton implanted at 10^{11} i/cm^2 in UO_2

Table 1 – Sample preparation and implantations conditions

Sample Type	Preparation cond.	U/O	Ion	Implantation fluence (i/cm^2)	Name
Polycrystalline	A1 OP-U A2	[1.9996;1.9998]	800 keV Xe	(1.4±0.1).10^{11}	Xe11p-1b
				(1.5±0.2).10^{11}	Xe11p-1c
			500 keV Kr	(1.5±0.2).10^{11}	Kr11p
				(2.0±0.2).10^{12}	Kr12p-1a
				(2.0±0.2).10^{12}	Kr12p-1b
				(2.0±0.2).10^{12}	Kr12p-1c

A1: Annealing at 1700°C during 24 hours under Ar-5%H_2
OP-U: Polishing treatment
A2: Annealing at 1400°C during 4 hours under Ar-5%H_2

Measurements of the release rates of xenon and krypton were performed on the PIAGARA platform at the LP2i Bordeaux [50], [51]. In the Thermo-Desorption Spectrometry (TDS) setup, ultra-high vacuum conditions are set (typically of 10^{-9} mbar before sample heating and up to 10^{-6} mbar at the end of an annealing under the static vacuum conditions). The setup comprises (i) the heating chamber (Mo furnace) including the sample placed in a platinum crucible, (ii) various calibrated volumes containing chemical traps allowing for gas samplings and purification, (iii) a calibrated monoisotopic reference gas for the quantitative calibration and (iv) the multicollector mass spectrometer measuring isotopic ratios. The Mo furnace is expected to act as an O getter. The calculations of O_2 potential equilibrium reveals that the maximum stoichiometry of the samples amounts to ~2.002 and according to Guéneau et al. [52], the samples cannot reach substantial under-stoichiometry for our working temperatures. Nonetheless, UO_2 samples are dropped in the furnace that is already heated to the desired temperature, limiting the deviation from stoichiometry of the samples.

Samplings and analyses are made every 20 minutes, which is the minimum time span to expand gas samplings, do the spectrometry analysis and pump the analyzed gas. Release curves are constructed from successive analyses of the cumulated gas releases. Each individual point obtained by TDS has an uncertainty related to mass spectrometry measurements. We minimize the errors mainly by adding precisely calibrated gas spikes of ^{82}Kr or ^{131}Xe to the gas samplings containing only ^{83}Kr or ^{129}Xe

isotopes. By checking the most abundant ^{84}Kr and ^{132}Xe isotopes, we also checked and if needed corrected any atmospheric contamination (either by micro-leaks or "memory" effects). The overall mass spectrometry measurement error for each data point was usually ranging 2-4%. This is significantly below the estimated ~±10% error on implantation fluence. The latter is thus considered as the dominant source of error and as such, is driving the final errors on the determined diffusion coefficients (see next Section).

Two annealing experiments were performed on both xenon and krypton implanted samples. The first with increasing temperatures from 600°C to 1400°C and the second with decreasing temperatures from 1350 or 1300°C to 1200°C or 1150°C. The samples were not removed from the vacuumed chamber during temperature changes. For each temperature, the isothermal release rate was measured and simulated by the following diffusion model.

3 Diffusion model

The diffusion model applied to the isotherms obtained at various temperatures is well described in previous work [30]. This model is based on Fick's second law and consider the trapping effect of gas atom (i) during the ion implantation process, associated to radiation induced damages and (ii) along the gas diffusion path by vacancy related defects. In this paper, the trapping mechanism during the implantation process will not be quantitatively effective since the samples used are implanted at low doses, below $1.4x10^{13}$ i/cm^2. This model also proposes an analytical form for the release by burst (discussed in previous work [30]) and is described as an equilibrium state mechanism where a high fraction of the mobile gas is released from the sample at the beginning of the annealing. Note that the burst probably depends on the surface [28], [53], grain boundaries [25], porosity [54], stoichiometry [43], [53], [55], [56], and is thermally activated [33], [53], [54], [57]. An extensive separated effect study would be necessary to investigate the mechanism of the burst release. Its consideration in our model nonetheless allows the determination of the gas loss during the burst, providing a better approximation of the evolution of the gas profile in UO_2 and thus, a more accurate determination of the diffusion coefficient.

According to Sabioni et al. [58] and Y. Ma [59], the surface of UO_2 sample annealed at 1350°C could evaporate under vacuum (condition required by the mass spectrometry measurements). This represents another route for Kr and Xe release by TDS that is necessary to take into account in the model. Evaporation rate at 1300°C and above was estimated from the following relation [60]:

$$R_{eva} = P_{sat(T)} \sqrt{\left(\frac{M_W}{2\pi RT}\right)} \quad (1)$$

where R_{eva} is the sublimation rate in kg/m^2/s, $P_{sat(T)}$ (in Pa) is the saturated vapour pressure for UO_2 for a given temperature ($P_{sat(T)}$ data deduced from the work by Ackermann et al. [61]), M_W is the UO_2 molecular weight (0.270 kg/mol), R is the universal gas constant (8.134 J/K/mol) and T is the temperature in K. On another project [62], this predictive model and its associated $P_{sat(T)}$ input data was confronted with measurements of mass difference before and after annealing: the model and the weight measurement agree well with a difference of only ~15% erosion rate. The evaporation rate at 1300, 1350 and 1400°C is calculated at 0.13, 0.52 and 1.67 pm/s by the model. Taking in consideration that in our experimental conditions erosions are rather low, the error on R_{eva} will merely propagate to the error associated to the final Xe or Kr diffusion rate.

The diffusion equation used in this work is as follows:

$$\begin{aligned}\frac{\partial C_m(x,t)}{\partial t} &= -B(t)\times C_m(x,t) + \frac{\partial}{\partial x}\left(D\frac{\partial C_m(x,t)}{\partial x}\right) - A(x)\times C_m(x,t) \\ &\quad - v_{eva}\frac{\partial C_m(x,t)}{\partial x} \\ \frac{\partial C_t(x,t)}{\partial t} &= A(x)\times C_m(x,t) + v_{eva}\frac{\partial C_t(x,t)}{\partial x}\end{aligned} \quad (2)$$

Where $C_m(x,t)$(m^{-3}) is the mobile gas concentration in the sample at a depth x and a time t, $B(t)$ is the burst release defined by eq.(3), D (m^2/s) is the diffusion coefficient, $A(x)$ is the frequency of the trapping along the gas diffusion path defined by eq.(4), v_{eva} (m/s) is the evaporation rate and $C_t(x,t)$ (m^{-3}) is the trapped gas concentration.

$$B(t) = \nu_b \times e^{-t/\tau} \quad (3)$$

Where ν_b(s^{-1}) is the burst frequency and τ (s) is its characteristic duration. The burst phenomenon is considered negligible after 5τ.

$$A(x) = \nu_t \times DPn(x) \quad (4)$$

Where ν_t (s^{-1}) is the trapping rate defined as $4\pi.r_t.T.D$ where r_t(m) is the trap equivalent radius, T (m^{-3}) is the concentration of traps, $DPn(x)$ is the normalized damage profile from SRIM calculations (Fig. 1). The trapping rate $A(x)$ is based on the assumption that it is diffusion-driven and has a depth dependency.

To determine the diffusion coefficient as a function of the temperature, each isotherm obtained at the temperature T_i is simulated independently. The initial gas content profile $C_m(x,0)[T_i]$ and $C_t(x,0)[T_i]$ are defined by the profiles obtained at the end of the previous annealing $C_m(x,t_{final})[T_{i-1}]$ and $C_t(x,t_{final})[T_{i-1}]$. The initial conditions for each isotherm are as follows:

$$\begin{aligned} &C_m(x,0)[T_0] = C_{SRIM}(x) \\ &C_t(x,0)[T_0] = 0 \\ \\ &C_m(x,0)[T_i] = C_m(x,t_{final})[T_{i-1}] \\ &C_t(x,0)[T_i] = C_t(x,t_{final})[T_{i-1}] \end{aligned} \quad (5)$$

Where $C_{SRIM}(x)$(m^{-3}) is the calculated profile of the gas content by the SRIM software (Fig. 1).

The boundaries equations are:

$$\begin{aligned} &C_m(0,t) = 0 \\ &C_m(x,t) = 0\,, \quad for\ x \geq 10\ \mu m \\ &C_t(0,t) = 0 \\ &C_t(x,t) = 0\,, \quad for\ x \geq 10\ \mu m \end{aligned} \quad (6)$$

The released fraction for each isotherm is calculated as the ratio between the amount of released gas content and the initial gas content:

$$f_{sim}(t)[i] = \frac{\int_{x=0}^{x_\infty} C_{SRIM}(x,0)[T_i] - \int_{x=0}^{x_\infty}\left[C_m(x,t)[T_i] + C_t(x,t)[T_i]\right]}{\int_{x=0}^{x_\infty} C_{SRIM}(x)dx} \quad (7)$$

The system of differential equations (2) is solved by finite element analysis using the FlexPDE program [https://www.pdesolutions.com/]. The optimization of the parameters is done with the *kmpfit* module of the python *kapteyn* library [63]. The simulations output the parameters $D[T_i]$, $\nu_t[T_i]$, $\nu_b[T_i]$, $\tau[T_i]$ and $v_{eva}[T_i \geq 1300°C]$ and the associated standard deviations for each isotherm. The dominant

error for these output parameters comes from the uncertainty on the estimated ion implantation fluences (±10%). One way to include the fluence fluctuation of 10% on the fit parameters errors is to evaluate the maximum variation of the parameters by fixing the fluence to the highest and lowest values. Therefore, three calculations were made for each sample: one at the fluence F, the second at the fluence $F + 0.1F$ and the third at the fluence $F - 0.1F$. These calculations give the maximum variation of the diffusion coefficient around 12% that is quadratically added to the standard deviation.

4 Results

Fig. 2 and Fig. 3 show the fractional release of xenon and krypton implanted at low concentration in UO_2 polycrystalline samples. Fig. 2 displays the experiment performed with increasing temperatures, from 600 to 1400°C and Fig. 3 show experiments performed with decreasing temperature, from 1350 or 1300°C to 1200 or 1150°C.

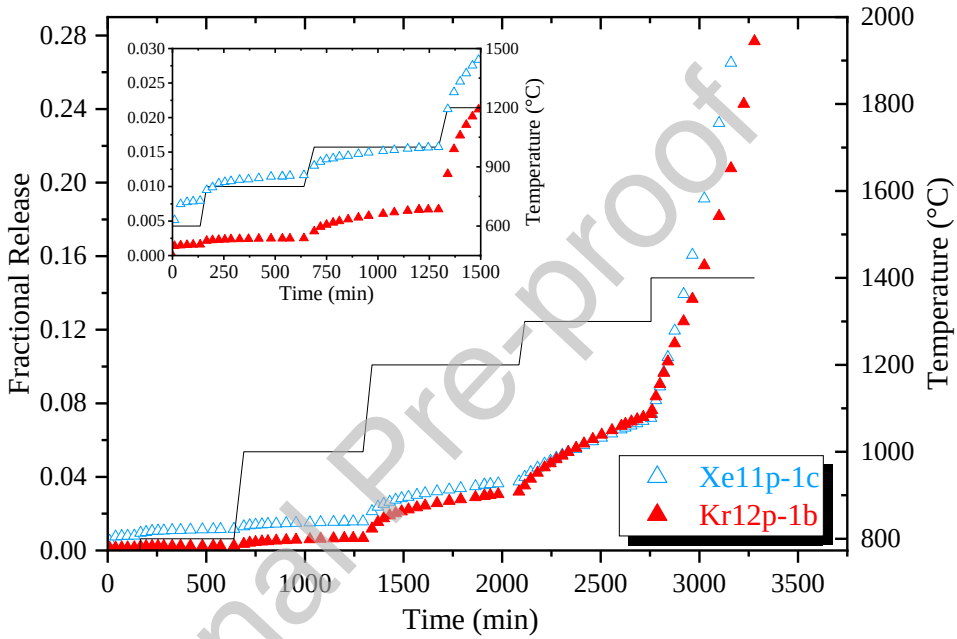

Fig. 2 – Fractional releases of Xe11p-1c implanted at 1.5x10^{11} i/cm^2 and of Kr12p-1b implanted at 2.0x10^{12} i/cm^2 in UO_2 annealed at temperatures ranging from 600 to 1400°C.

*Table 2 – Simulation parameters from fractional release of xenon implanted at 1.5x10^{11} i/cm^2 and of krypton implanted at 2.0x10^{12} i/cm^2 in UO_2 annealed at temperatures ranging from 1200 to 1400°C. Some values, marked with *, are fixed in the simulation because of the high number of variables. Due to the shape of gas release at 1400°C, we found reasonable to neglect the burst release and the trapping, improving the precision on the other parameters. At 1300°C, the evaporation rate was settled at 0.13 pm/s (see eq.(1), section 3).*

Ion	Name	T (°C)	t_{final} (min)	ν_b $(\times 10^{-5} s^{-1})$	τ (s)	D $(\times 10^{-20} m^2/s)$	ν_t $(\times 10^{-5} s^{-1})$	ν_{eva} $(\times 10^{-12} m/s)$
800 keV Xe	Xe11p-1c (1.5x10^{11})	1200	790	0.23 ± 0.01	4676 ± 94	0.41 ± 0.05	< 1.5	0*
		1300	670	0.09 ± 0.01	7252 ± 286	1.11 ± 0.13	< 1.5	0.13*
		1400	525	0*	1*	7.64 ± 0.92	0*	1.85 ± 0.07
500 keV Kr	Kr12p-1b (2.0x10^{12})	1200	790	0.22 ± 0.01	5628 ± 252	0.38 ± 0.05	< 1.5	0*
		1300	670	0.14 ± 0.01	10041 ± 748	0.93 ± 0.11	< 1.5	0.13*
		1400	525	0*	1*	5.75 ± 0.87	0*	1.20 ± 0.18

For temperatures at 1000°C and below, release by diffusion is extremely low (totaling less than 1.5‰), with a major contribution of release through burst effect (above 50% of the total release – potentially 100% at 600°C). If the analytical form of the burst is not a plateau but rather a diffusive phenomenon, its contribution over the time might be slightly underestimated, having a high impact on the determination of the diffusion coefficient on such low release rates. It is therefore not reasonable to interpret the modeling results on these "burst-impaired" releases. At temperatures from 1200°C, the

gas release reaches 2% (Xe or Kr) and the burst contribution is weaker (below 45% of the total release) so the hypothetical influence of a diffusive form of the burst becomes negligible. That is why Table 2 presents the simulation parameters obtained only from fractional releases at temperatures ranging from 1200 to 1400°C.

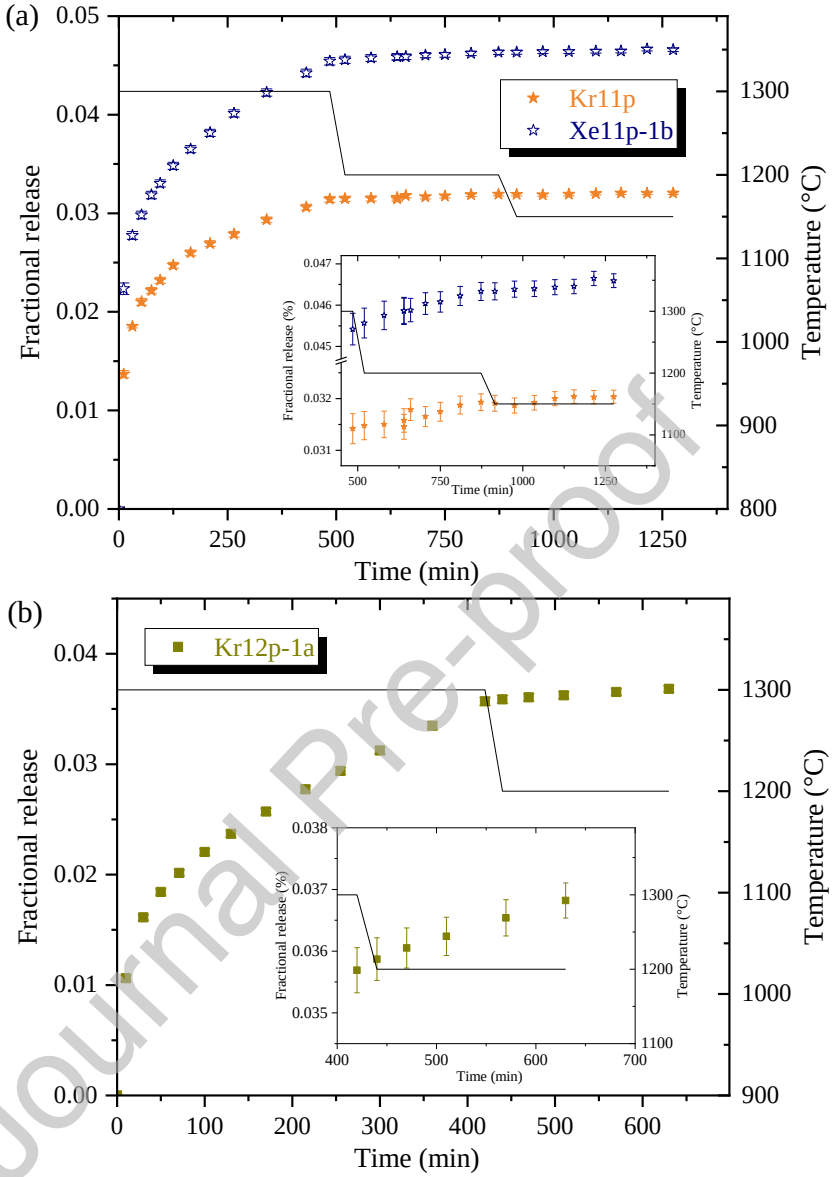

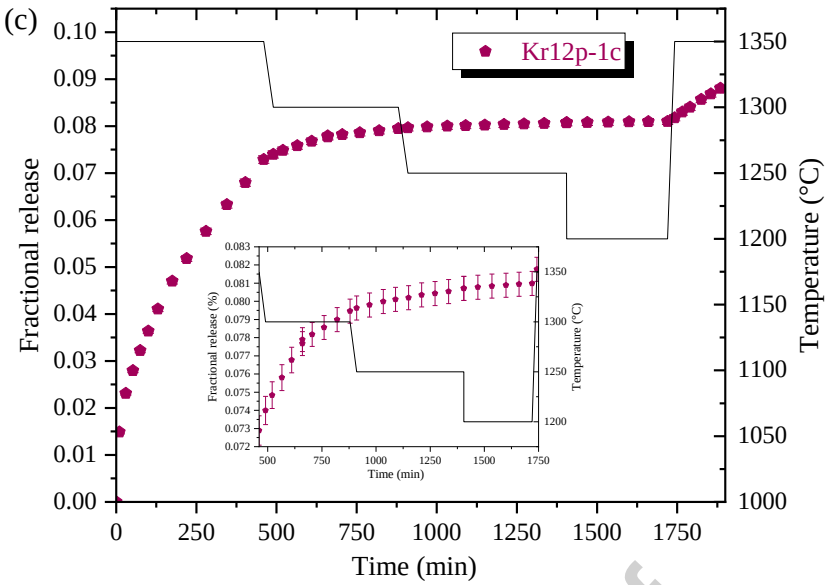

Fig. 3 – Fractional releases of (a) xenon implanted at 1.4x10^{11} i/cm^2 and of krypton implanted at 1.5x10^{11} i/cm^2 in UO_2 annealed at temperatures ranging from 1300 to 1150°C, (b) krypton implanted at 2.0x10^{12} i/cm^2 in UO_2 annealed at temperatures ranging from 1300 to 1200°C and (c) krypton implanted at 2.0x10^{12} i/cm^2 in UO_2 annealed at temperatures ranging from 1350 to 1200°C

*Table 3 – Simulation parameters from release rates at temperatures ranging from 1350 or 1300°C to 1200 or 1150°C of low doses 800 keV Xe or 500 keV Kr implanted in UO_2 samples. Note that some of the samples presented here were used in our former study on Xe diffusion at 1300°C [30]. Because of the upgrade of the fitting program, the value on the diffusion coefficient changed but remained in the former values' error bars. Fixed values are marked with *.*

Ion	Name	T (°C)	t_{final} (min)	ν_b ($\times 10^{-5} s^{-1}$)	τ (s)	D ($\times 10^{-20} m^2/s$)	ν_t ($\times 10^{-5} s^{-1}$)	v_{eva} ($\times 10^{-12} m/s$)
800 keV Xe	Xe11p-1b (1.4x10^{11})	1300	485	6.88 ± 0.24	370 ± 13	2.19 ± 0.28	6.64 ± 0.22	0.13*
		1200	388	0*	1*	0.36 ± 0.16	< 3	0*
		1150	402	0*	1*	0.14 ± 0.10	< 3	0*
500 keV Kr	Kr12p-1a (2.0x10^{12})	1300	420	2.41 ± 0.08	601 ± 21	1.41 ± 0.17	3.31 ± 0.14	0.13*
		1200	210	0*	1*	0.23 ± 0.10	< 3	0*
	Kr11p (1.5x10^{11})	1300	485	3.35 ± 0.21	498 ± 32	1.43 ± 0.20	8.77 ± 0.50	0.13*
		1200	388	0*	1*	0.33 ± 0.17	< 3	0*
		1150	402	0*	1*	0.12 ± 0.11	< 3	0*
	Kr12p-1c (2.0x10^{12})	1350	460	3.36 ± 0.17	493 ± 36	4.43 ± 0.57	5.91 ± 0.24	0.52*
		1300	420	0*	1*	1.68 ± 0.61	< 3	0.13*
		1250	525	0*	1*	0.33 ± 0.23	< 3	0*
		1200	315	0*	1*	0.14 ± 0.41	< 3	0*
		1350	308	0*	1*	4.80 ± 0.67	0*	0.26 ± 0.01

For annealings with increasing temperatures, we observe a burst release at each temperature plateau up to 1300°C. For annealings with decreasing temperatures however, the release by burst only occurs at the first annealing. For the following annealings at lower temperatures, the absence of burst greatly increases the accuracy of the simulation of the release profiles, hence the precision of *D* determination. At 1150°C, the fractional release rate is extremely low (~1 ‰ for few hours) and therefore represents the lower limit of our analysis possibilities.

The simulations obtained on annealings with increasing temperatures show that the burst effect occurs at each temperature step from 600°C to 1200°C but not at 1300°C (see Table 3). This means that at this point, the release by burst is negligible compared to release by diffusion. Previous work showed however the burst release at 1300°C from annealing experiments performed directly at this temperature (no annealing at lower temperature before) [30]. The burst at 1300°C is also clearly distinguished on the experiments displayed on Fig. 3(a) and Fig. 3(b) where 1300°C is the first temperature step. When the first annealing is performed at 1300°C, the burst release at this temperature concerns 1.5 to 2.8% of xenon content and 1.4 to 1.8% of krypton content. Between 600

and 1200°C, 2.2% of xenon and 1.8% of krypton are cumulatively released by burst. This observation tends to prove that gas atoms released by burst are held in some kind of reservoir, releasing parts of this mobile gas population depending on temperature. One might rise the assumption that the burst release is associated to the thermal dependence of the mobility of various kind of defects. Microstructural characterisations are required to identify the nature of the so-called reservoir.

On annealings with increasing temperatures, we estimated the limit value of the trapping parameter ν_t as 1.5×10^{-5} s^{-1}. Below this value, the trapping influence on the diffusion is too low and the model cannot output a reliable ν_t value. According to Table 3, ν_t does not exceed this limit. On annealings with decreasing temperatures (see Fig. 3), the fractional release of xenon and krypton are very low at temperatures lower than 1250°C, which induce relatively high uncertainties on the diffusion coefficient (Table 3). As a consequence, the model cannot output reasonable values on ν_t. We evaluated that for a diffusion coefficient of about 10^{-21} m^2/s, the limit values of ν_t reaches 3.10^{-5} s^{-1}. ν_t is evaluated with good accuracy for the temperatures of 1350 and 1300°C (Table 3), however this is insufficient for assessing the trapping frequency dependence with the temperature.

On sample Kr12p-1c, a second annealing at 1350°C was performed after annealings with decreasing temperatures (see Fig. 3(c)). The diffusion coefficient values obtained on both 1350°C annealings are in good agreement although the first is simulated with the burst and the second without (all the burst population is evacuated during the first annealing at 1350°C). This result means that, considering its sensitivity, the model is representative of the evolution of the gas profile during the various annealings and that the burst modelling complicates but does not impair and refine the determination of the diffusion coefficient.

At 1300°C, diffusion coefficients values for xenon and krypton are in good agreement with a previous work we carried out on xenon and krypton diffusion in implanted UO_2. The diffusion coefficient at 1300°C was found to be $(1.73 \pm 0.15) \times 10^{-20}$ m^2/s.

5 Arrhenius law of xenon and krypton implanted in UO_2

Following the in-pile study of Turnbull et al. [64], the diffusion above 1200°C is driven by a thermal process. It is defined by $D^{thermal}(T)$ and is expressed by the Arrhenius law for thermally activated processes as:

$$D^{thermal}(T) = D_0 exp\left(\frac{-E_a}{k_B T}\right) \quad (8)$$

where E_a is the activation energy and D_0 is the pre-exponential factor. Also in the study of Turnbull et al. [64], the diffusion below 1200°C is assisted by radiation damage. Since this work is performed on implanted UO_2 samples at very low concentrations, we do not expect radiation damage to control the diffusion below 1200°C.

Diffusion coefficients as a function of 1/T from the two annealing experiments (increasing and decreasing temperatures) are plotted in Fig. 4. Xenon and krypton diffusion coefficients are overall very close at each temperature, independently of increasing or decreasing temperature annealings. This proves that the modelling of the burst as an equilibrium state mechanism is relevant here. Also, Fig. 4 suggests that both gases probably diffuse by the same mechanisms, meaning that the diffusion mechanism in UO_2 is quantitatively independent of atomic mass or radius.

In order to obtain the activation energy and pre-exponential factor, an exponential fit is performed (error weighted) either on concatenated data or on each individual annealing experiment. Each conditions and the associated E_a et D_0 values are presented in Table 4. Considering the uncertainty on

E_a and the close values on D_0, one cannot distinguish Arrhenius laws depending on the fitting choice. The agreement on the E_a et D_0 values shows the reproducibility of the method on samples implanted with either Xe or Kr at fluences lower than 5.10^{13} i/cm^2, annealed with increasing or decreasing temperatures. The dotted red line in Fig. 4 represents the fit on all concatenated data.

Table 4 – E_a and D_0 determined depending on the simulation choice

		E_a (eV)	D_0 (m^2/s)
Concatenated Data	All	3.16 ± 0.27	$1.83^{9.1}_{0.4} \times 10^{-10}$
	Xe only	3.26 ± 0.35	$3.73^{27.0}_{0.4} \times 10^{-10}$
	Kr only	3.04 ± 0.51	$8.11^{200.0}_{0.8} \times 10^{-11}$
Individual fits	Mean Value - All	3.04 ± 0.36	$1.56^{100.0}_{0.6} \times 10^{-11}$

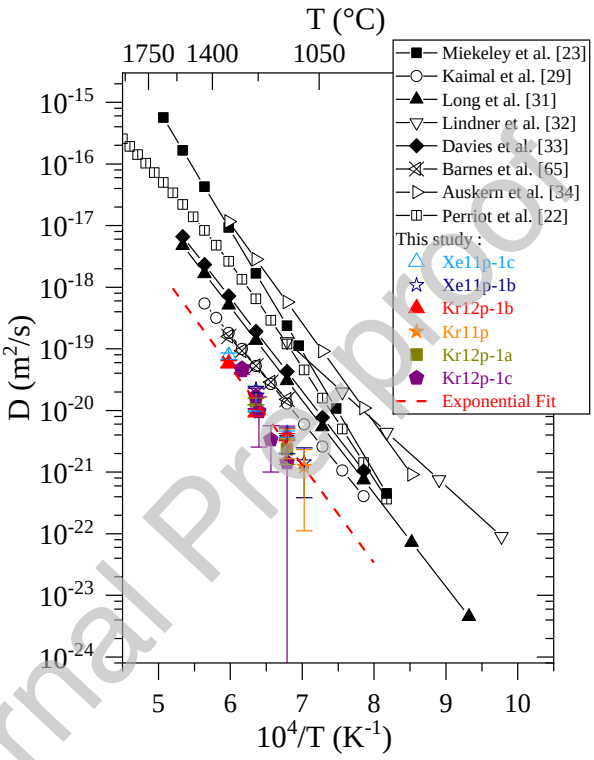

Fig. 4 – Temperature dependence on diffusion coefficients of xenon and krypton in polycrystalline UO_2. Annealing experiments from 1200 to 1400°C and from 1350 to 1150°C. The dotted red line represents the exponential fit on concatenated data. Error bars on the x axis (temperature) are covered by the size of the symbols.

The activation energy and pre-exponential factor values show a good agreement with literature studies of xenon diffusion in low irradiated near stoichiometric UO_2 in the same temperature range ($2.1 < E_a < 3.9$ eV and $2.10^{-12} < D_0 < 5.10^{-4}$ m^2/s) [22], [23], [28], [31]–[34], [65].

The recent study of Horlait et al. [26] describes a device that enables O_2 addition into the heating chamber (where the UO_2 pellet stands). The first results show that a slight increase of x in UO_{2+x} from a starting supposedly perfectly stoichiometric UO_2 could drastically change the diffusion coefficient of Kr (e.g. a D_{Kr} increase by one order of magnitude for an x increase of only 0.001), but merely change the activation energy. The scattered data outlined in Fig. 4, although the corresponding studies agrees rather well on E_a, is thus explained by slight and undiscernible variations on the uranium dioxide stoichiometry between studies (either from slightly different oxygen partial pressure conditions and/or impurity effects). This assumption is also supported by extended results to be published [62].

6 Conclusion

The thermal diffusion of rare gases implanted at low fluences in uranium dioxide has been investigated. Annealing experiments under vacuum at various temperatures were performed to obtain isothermal release rate measurements. The latter were simulated with a diffusion model based on the Fick's second law with the aim of evaluating the diffusion mechanisms. First, we identified the burst effect (occurring at the beginning of some annealing experiments) as the release of gas atoms from a specific reservoir. When the reservoir is empty – by an annealing at a high temperature (1350 or 1300°C) or by successive annealing at lower temperature(s) – the burst effect is not observed.

Secondly, it was found that xenon and krypton diffuse by the same mechanisms and kinetics, at least for the fluence and temperature ranges explored here. Although its simplicity compared to the realistic conditions, the model defined in this work shows its relevance to represents major evolution on the gas diffusion profiles. Good agreement was found with previous studies on the activation energy (E_a = 3.2±0.3 eV) and pre-exponential factor (D_0 between 0.4×10^{-10} and 9.1×10^{-10} m^2/s) in the thermal diffusion regime.

Finally, this study intends to contribute to the improvement of performance codes that are developed to simulate the fuel behaviour in-pile [66], [67]. An extensive review of performance codes for LWR fuel application can be found in [68]. Multiple codes are developed to specifically simulate the fission gas release from UO_2 as for example SFPR [69], FASTGRASS [70], SCIANTIX [71], CARACAS and MARGARET in ALCYONE [72], [73] or SIFGRS in BISON [40].

Acknowledgments

This research is part of the INSPYRE project, which has received funding from the Euratom research and training program 2014-2018 under Grant Agreement No 754329. We thank Anthony Duranti (IP2I/IN2P3 CNRS) for Xe and Kr implantation and Claire Onofri (CEA/DEN) for uranium dioxide pellets fabrication.

References

[1] H. Bailly, D. Ménissier, and C. Prunier, *Le combustible nucléaire des réacteurs à eau sous pression et des réacteurs à neutrons rapides, conception et comportement*, CEA, Eyrolles, Série synthèse. 1996.

[2] M. Tonks *et al.*, "Unit mechanisms of fission gas release: Current understanding and future needs," *J. Nucl. Mater.*, vol. 504, pp. 300–317, Jun. 2018, doi: 10.1016/j.jnucmat.2018.03.016.

[3] J. Rest, M. W. D. Cooper, J. Spino, J. A. Turnbull, P. Van Uffelen, and C. T. Walker, "Fission gas release from UO2 nuclear fuel: A review," *J. Nucl. Mater.*, Aug. 2018, doi: 10.1016/j.jnucmat.2018.08.019.

[4] Hj. Matzke, "Gas release mechanisms in UO2 - A critical review," *Radiat. Eff.*, vol. 53, pp. 219–242, 1980.

[5] D. A. Andersson, B. P. Uberuaga, P. V. Nerikar, C. Unal, and C. R. Stanek, "U and Xe transport in UO 2 ± x : Density functional theory calculations," *Phys. Rev. B*, vol. 84, no. 5, 2011, doi: 10.1103/PhysRevB.84.054105.

[6] X.-Y. Liu, B. P. Uberuaga, D. A. Andersson, C. R. Stanek, and K. E. Sickafus, "Mechanism for transient migration of xenon in UO2," *Appl. Phys. Lett.*, vol. 98, p. 151902, 2011.

[7] J.-P. Crocombette, "Ab initio energetics of some fission products (Kr, I, Cs, Sr and He) in uranium dioxide," *J. Nucl. Mater.*, vol. 305, no. 1, pp. 29–36, 2002.

[8] M. Freyss, N. Vergnet, and T. Petit, "Ab initio modeling of the behavior of helium and xenon in actinide dioxide nuclear fuels," *J. Nucl. Mater.*, vol. 352, no. 1–3, pp. 144–150, Jun. 2006, doi: 10.1016/j.jnucmat.2006.02.048.

[9] T. Petit *et al.*, "Molecular modelling of transmutation fuels and targets," *J. Nucl. Mater.*, vol. 320, no. 1–2, pp. 133–137, Jul. 2003, doi: 10.1016/S0022-3115(03)00179-X.

[10] T. Petit, G. Jomard, C. Lemaignan, B. Bigot, and A. Pasturel, "Location of krypton atoms in urnaium dioxide," *J. Nucl. Mater.*, vol. 275, pp. 119–123, 1999.
[11] A. E. Thompson and C. Wolverton, "First-principles study of noble gas impurities and defects in UO 2," *Phys. Rev. B*, vol. 84, no. 13, Oct. 2011, doi: 10.1103/PhysRevB.84.134111.
[12] Y. Yun, H. Kim, H. Kim, and K. Park, "Atomic diffusion mechanism of Xe in UO2," *J. Nucl. Mater.*, vol. 378, no. 1, pp. 40–44, Aug. 2008, doi: 10.1016/j.jnucmat.2008.04.013.
[13] Y. Yun, O. Eriksson, P. M. Oppeneer, H. Kim, and K. Park, "First-principales theory for helium and xenon diffusion in uranium dioxide," *J. Nucl. Mater.*, vol. 385, pp. 364–367, 2009.
[14] P. V. Nerikar, X.-Y. Liu, B. P. Uberuaga, C. R. Stanek, S. R. Phillpot, and S. B. Sinnott, "Thermodynamics of fission products in UO2±x," *J. Phys. Condens. Matter*, vol. 21, no. 43, p. 435602, Oct. 2009, doi: 10.1088/0953-8984/21/43/435602.
[15] E. Vathonne *et al.*, "Determination of Krypton Diffusion Coefficients in Uranium Dioxide Using Atomic Scale Calculations," *Inorg. Chem.*, vol. 56, no. 1, pp. 125–137, Jan. 2017, doi: 10.1021/acs.inorgchem.6b01560.
[16] D. A. Andersson *et al.*, "Atomistic modeling of intrinsic and radiation-enhanced fission gas (Xe) diffusion in UO2±x : Implications for nuclear fuel performance modeling," *J. Nucl. Mater.*, vol. 451, no. 1–3, pp. 225–242, Aug. 2014, doi: 10.1016/j.jnucmat.2014.03.041.
[17] R. W. Grimes and C. R. A. Catlow, "The Stability of Fission Products in Uranium Dioxide," *Philos. Trans. R. Soc. Math. Phys. Eng. Sci.*, vol. 335, no. 1639, pp. 609–634, Jun. 1991, doi: 10.1098/rsta.1991.0062.
[18] K. Govers, S. E. Lemehov, and M. Verwerft, "On the solution and migration of single Xe atoms in uranium dioxide – An interatomic potentials study," *J. Nucl. Mater.*, vol. 405, no. 3, pp. 252–260, Oct. 2010, doi: 10.1016/j.jnucmat.2010.08.013.
[19] S. T. Murphy, A. Chartier, L. Van Brutzel, and J.-P. Crocombette, "Free energy of Xe incorporation at point defects and in nanovoids and bubbles in UO 2," *Phys. Rev. B*, vol. 85, no. 14, Apr. 2012, doi: 10.1103/PhysRevB.85.144102.
[20] S. Nicoll, H. Matzke, and C. R. A. Catlow, "A computational study of the effect of Xe concentration on the behaviour of single Xe atoms in UO2," *J. Nucl. Mater.*, vol. 226, no. 1–2, pp. 51–57, 1995.
[21] M. W. D. Cooper, C. R. Stanek, J. A. Turnbull, B. P. Uberuaga, and D. A. Andersson, "Simulation of radiation driven fission gas diffusion in UO 2 , ThO 2 and PuO 2," *J. Nucl. Mater.*, vol. 481, pp. 125–133, Dec. 2016, doi: 10.1016/j.jnucmat.2016.09.013.
[22] R. Perriot, C. Matthews, M. W. D. Cooper, B. P. Uberuaga, C. R. Stanek, and D. A. Andersson, "Atomistic modeling of out-of-pile xenon diffusion by vacancy clusters in UO2," *J. Nucl. Mater.*, vol. 520, pp. 96–109, Jul. 2019, doi: 10.1016/j.jnucmat.2019.03.050.
[23] W. Miekeley and F. W. Felix, "Effect of stoichiometry on diffusion of xenon in UO2," *J. Nucl. Mater.*, vol. 42, no. 3, pp. 297–306, Mar. 1972, doi: 10.1016/0022-3115(72)90080-3.
[24] J. Linder and P. Spindler, "Diffusion of Xenon 1300 in UO2 Single Crystals," *Z Naturforschg*, vol. 21a, pp. 1723–1725, 1966.
[25] K. Une, K. Nogita, S. Kashibe, and M. Imamura, "Microstructural change and its influence on fission gas release in high burnup UO2 fuel," *J. Nucl. Mater.*, vol. 188, pp. 65–72, 1992.
[26] D. Horlait *et al.*, "A new thermo-desorption laser-heating setup for studying noble gas diffusion and release from materials at high temperatures," *Rev. Sci. Instrum.*, vol. 92, no. 12, p. 124102, Dec. 2021, doi: 10.1063/5.0068858.
[27] J. R. MacEwan and W. H. Stevens, "Xenon Diffusion in UO2 - Some Complicating Factors," *J. Nucl. Mater.*, vol. 11, no. 1, pp. 77–93, 1964.
[28] K. N. G. Kaimal, M. C. Naik, and A. R. Paul, "Effect of irradiation and dopant concentration on the migration of xenon in UO2," *Met. Mater. Process.*, vol. 1, pp. 293–300, 1990.
[29] K. N. G. Kaimal, M. C. Naik, and A. R. Paul, "Temperature dependence of diffusivity of xenon in high dose irradiated UO 2," *J. Nucl. Mater.*, vol. 168, no. 1, pp. 188–190, 1989.
[30] M. Gerardin, E. Gilabert, D. Horlait, M.-F. Barthe, and G. Carlot, "Experimental study of the diffusion of Xe and Kr implanted at low concentrations in UO2 and determination of their trapping mechanisms," *J. Nucl. Mater.*, vol. 556, p. 153174, Dec. 2021, doi: 10.1016/j.jnucmat.2021.153174.

[31] Long, G, Davies, D, and J. R. Findlay, "Diffusion of Fission Products in Uranium Dioxide and uranium Monocarbide," *UKAEA Memo AERE-M1251*, 1964.
[32] R. Lindner and Hj. Matzke, "Diffusion von Xe-133 in Uranoxyd verschiedenen Sauerstoffgehaltes," *Z Naturforschg*, no. 14a, pp. 582–584, 1959.
[33] D. Davies and G. Long, "The emission of xenon-133 from lightly irradiated uranium dioxide spheroids and powders.," vol. AERE-R 4347, 1963.
[34] A. B. Auskern, "The diffusion of krypton 85 from uranium dioxide powder," *US Rep. WAPD-TM-185*, 1960.
[35] A. H. Booth and G. T. Rymer, "Determination of the Diffusion Constant of Fission Xenon on UO2 Crystals and Sintered Compacts," *AECL-CRDC-720*.
[36] A. Sy Ong and S. Elleman, "Effect or trapping in the release of recoil injected gases from solids," *Nucl. Instrum. Methods*, vol. 86, pp. 117–125, 1970.
[37] M. V. Speight, "A Calculation on the Migration of Fission Gas in Material Exhibiting Precipitation and Re-solution of Gas Atoms Under Irradiation," *Nucl. Sci. Eng.*, vol. 37, no. 2, pp. 180–185, Aug. 1969, doi: 10.13182/NSE69-A20676.
[38] F. S. Ham, "Theory of Diffusion-Limited Precipitation," *J Phys Chem Solids*, vol. 6, pp. 335–351, 1958.
[39] R. M. Cornell, M. V. Speight, and B. C. Masters, "The role of bubbles in fission gas release from uranium dioxide," *J. Nucl. Mater.*, vol. 30, no. 1–2, pp. 170–178, 1969.
[40] R. J. White and M. O. Tucker, "A new Fission-Gas Release Model," *J. Nucl. Mater.*, vol. 118, pp. 1–38, 1983.
[41] P. W. Winter and D. A. MacInnes, "An Analysis of the Thermodynamics of Gas Atoms in very small Bubbles," *J. Nucl. Mater.*, vol. 114, pp. 7–14, 1983.
[42] P. T. Elton, P. E. Coleman, and D. A. MacInnes, "A Mechanism for Fission Gas Release from High Temperature Fuel," *J. Nucl. Mater.*, vol. 135, pp. 63–67, 1985.
[43] J. C. Carter, E. J. Driscoll, and T. S. Elleman, "Xenon-133 diffusion and trapping in single crystal uranium dioxide," *Phys Stat Sol A*, vol. 14, pp. 673–680, 1972.
[44] "Active Oxide Polishing Suspensions - Brochure." Struers, 2006.
[45] D. Zipperian, "Colloidal Silica Polishing." PACE Technologies - Quality Matters Newsletter, 2003.
[46] S. Massara and C. Guéneau, "Thermodynamics of Advanced Fuels – International Database," vol. NEA News, no. 32, p. 24, 2014.
[47] J. F. Ziegler, J. P. Biersack, and U. Littmark, "The stopping and Range of Ions in Matter," 2008.
[48] J. Soullard and A. Alamo, "Study on Deceleration of Ions in Diatomic Target," *Radiat. Eff.*, vol. 38, p. 113, 1978.
[49] J. Soullard, "High voltage electron microscope observations of UO2," *J. Nucl. Mater.*, vol. 135, no. 2–3, pp. 190–196, 1985.
[50] F. Linez, E. Gilabert, A. Debelle, P. Desgardin, and M.-F. Barthe, "Helium interaction with vacancy-type defects created in silicon carbide single crystal," *J. Nucl. Mater.*, vol. 436, pp. 150–157, 2013.
[51] A. Özgümüs, E. Gilabert, N. Dacheux, C. Tamain, and B. Lavielle, "Study of radiogenic helium diffusion in the β-thorium phosphate diphosphate ceramic," *J. Nucl. Mater.*, vol. 373, pp. 112–118, 2008.
[52] C. Guéneau, M. Baichi, D. Labroche, C. Chatillon, and B. Sundman, "Thermodynamic assessment of the uranium–oxygen system," *J. Nucl. Mater.*, vol. 304, no. 2, pp. 161–175, Aug. 2002, doi: 10.1016/S0022-3115(02)00878-4.
[53] K. Taketani, "Release of xenon from sintered UO2 at low temperatures".
[54] M. C. Naik, K. N. G. Kaimal, and M. D. Karkhanavala, "Release of xenon from low-dose irradiated thoria pellets," *J. Nucl. Mater.*, vol. 67, no. 3, pp. 239–243, 1977.
[55] J. H. Evans, A. Van Veen, and K. T. Westerduin, "An investigation into the influence of implanted oxygen on krypton behaviour in uranium dioxide during annealing," *J. Nucl. Mater.*, vol. 208, no. 3, pp. 211–218, 1994.
[56] W. H. Stevens and J. R. MacEwan, "The diffusion behavior of fission xenon in uranium dioxide," *At. Energy Can. Ltd. Chalk River Ont. Can.*, 1960.

[57] A. O. R. Cavaleru, D. G. Armour, and G. Carter, "Thermal evolution spectrometry of low energy inert gas ions injected into polycrystalline UO2," *Vacuum*, vol. 24, no. 1, pp. 13–21, 1973.
[58] A. C. S. Sabioni, W. B. Ferraz, and F. Millot, "First study of uranium self-diffusion in UO2 by SIMS," *J. Nucl. Mater.*, vol. 257, pp. 180–184, 1998.
[59] Y. Ma, "A study of point defects in UO2+x and their impact upon fuel properties," Aix-Marseille, 2017.
[60] E. L. Andreas, "New estimates for the sublimation rate for ice on the Moon," *Icarus*, vol. 186, no. 1, pp. 24–30, Jan. 2007, doi: 10.1016/j.icarus.2006.08.024.
[61] R. J. Ackermann, P. W. Gilles, and R. J. Thorn, "High-Temperature Thermodynamic Properties of Uranium Dioxide," *J. Chem. Phys.*, vol. 25, no. 6, pp. 1089–1097, Dec. 1956, doi: 10.1063/1.1743156.
[62] D. Horlait *et al.*, "Experimental diffusion of Kr in UO2+x as a function of stoichiometry: tiny stoichiometry deviations, great effects.," *J. Nucl. Mater.*, under review 2022.
[63] P. Terlouw and M. G. R. Vogelaar, "Kapteyn Package: Tools for developing astronomical applications, Astrophysics Source Code Library." 2016.
[64] Turnbull, "The diffusion coefficients of gaseous and volatile species during the irradiation of uranium dioxide," *J. Nucl. Mater.*, vol. 107, pp. 168–184, 1982.
[65] R. Barnes, "Xenon diffusion in single crystal and sintered UO2," *Rep. BMI 1533*, 1961.
[66] P. V. Uffelen, "Use of advanced simulations in fuel performance codes," *NEA/NSC/R*, vol. 5, p. 7, 2015.
[67] H. S. Aybar and P. Ortego, "A review of nuclear fuel performance codes," *Prog. Nucl. Energy*, vol. 46, no. 2, pp. 127–141, Jan. 2005, doi: 10.1016/j.pnucene.2005.01.004.
[68] P. Van Uffelen, J. Hales, W. Li, G. Rossiter, and R. Williamson, "A review of fuel performance modelling," *J. Nucl. Mater.*, vol. 516, pp. 373–412, Apr. 2019, doi: 10.1016/j.jnucmat.2018.12.037.
[69] M. S. Veshchunov, A. V. Boldyrev, V. D. Ozrin, V. E. Shestak, and V. I. Tarasov, "A new mechanistic code SFPR for modeling of single fuel rod performance under various regimes of LWR operation," *Nucl. Eng. Des.*, vol. 241, no. 8, pp. 2822–2830, Aug. 2011, doi: 10.1016/j.nucengdes.2011.05.032.
[70] J. Rest and S. A. Zawadzki, "FASTGRASS: A mechanistic model for the prediction of Xe, I, Cs, Te, Ba, and Sr release from nuclear fuel under normal and severe-accident conditions," NUREG/CR-5840, ANL--92/3, 7255051, Sep. 1992. doi: 10.2172/7255051.
[71] D. Pizzocri, T. Barani, and L. Luzzi, "SCIANTIX: A new open source multi-scale code for fission gas behaviour modelling designed for nuclear fuel performance codes," *J. Nucl. Mater.*, vol. 532, p. 152042, Apr. 2020, doi: 10.1016/j.jnucmat.2020.152042.
[72] A. Boulore, C. Struzik, R. Masson, P. Mailhe, and R. Largenton, "Approach to better assess fission gas behaviors, applicable to fuels with complex microstructures," p. 12, 2019.
[73] L. Noirot, "MARGARET: A comprehensive code for the description of fission gas behavior," *Nucl. Eng. Des.*, vol. 241, no. 6, pp. 2099–2118, Jun. 2011, doi: 10.1016/j.nucengdes.2011.03.044.

Credit Author Statement

Marie-France Barthe : Supervision. **Gaëlle Carlot** : Supervision, Methodology, Investigation, Project administration. **Denis Horlait** : Writing – Review & Editing, Investigation. **Eric Gilabert** : Writing – Review & Editing, Methodology, Software, Investigation, Formal analysis. **Marie Gerardin** : Writing – Original Draft, Writing – Review & Editing, Investigation.

Declaration of interests

☒ The authors declare that they have no known competing financial interests or personal

relationships that could have appeared to influence the work reported in this paper.

☐ The authors declare the following financial interests/personal relationships which may be considered as potential competing interests: